



Evaluation of thermal conductivity of organic phase-change materials from equilibrium and non-equilibrium computer simulations: Paraffin as a test case

Victor M. Nazarychev^a, Artyom D. Glova^a, Igor V. Volgin^a, Sergey V. Larin^a, Alexey V. Lyulin^{a,b}, Sergey V. Lyulin^a, Andrey A. Gurtovenko^{a,*}

^a Institute of Macromolecular Compounds, Russian Academy of Sciences, Bolshoi Prospect V.O. 31, St. Petersburg, 199004, Russia

^b Theory of Polymers and Soft Matter Group, Technische Universiteit Eindhoven, P.O. Box 513, 5600 MB Eindhoven, the Netherlands

ARTICLE INFO

Article history:

Received 22 July 2020

Revised 9 October 2020

Accepted 21 October 2020

Keywords:

Thermal conductivity
Phase-change materials
Paraffins
Computer modeling
Molecular dynamics

ABSTRACT

An accurate *in silico* evaluation of the thermal conductivity is critical for improving the thermal properties of organic phase-change materials on a rational basis. To explore the impact of a theoretical model on the computed thermal conductivity, here we employed the equilibrium and the non-equilibrium molecular dynamics (MD) simulations to study paraffin (n-eicosane) bulk samples, in both crystalline and liquid states, with the use of 10 atomistic force fields, both all-atom and united-atom ones. Overall, we found that the equilibrium MD method is preferable for computing the thermal conductivity of n-eicosane samples (at least for a 10-nm-size simulation box). For the n-eicosane crystals, the all-atom models provide larger thermal conductivity coefficients than their united-atom counterparts and, correspondingly, a better match with the experimental data. This is most likely because the crystalline lattice of the models with explicit hydrogen atoms is additionally stabilized by the electrostatic interactions. In contrast, in the liquid state, most all-atom models overestimate the experimental data for n-eicosane, providing thereby worse performance as compared to the united-atom force fields. However, when it comes to the experimentally observed increase in the thermal conductivity of n-eicosane samples upon crystallization, only all-atom models are able to reproduce quantitatively the experimental data. Each force field of n-eicosane was also characterized by an overall score which accumulated the deviations of the computed thermal conductivity coefficients from the experimental values, for both crystalline and liquid samples. It turns out that the best performance among 10 atomistic models of n-eicosane is observed for the all-atom GAFF force field. All in all, our study clearly demonstrates that a proper choice of the model for computing the thermal conductivity is a non-trivial task: even for such relatively simple compounds as paraffins (n-alkanes), different models perform quite differently, in equilibrium and in non-equilibrium MD simulations, as well as in crystalline and liquid phases.

© 2020 Elsevier Ltd. All rights reserved.

1. Introduction

Managing the heat transfer is an important issue in materials science, as it has critical impact on many practical applications such as heat storage systems, thermoelectric and photovoltaic devices [1–3]. For instance, paraffin-based phase-change materi-

als have an outstanding ability to store/release the thermal energy upon melting and crystallization [2]. However, practical applications of these materials are rather limited due to their low thermal conductivity [2,3]. One of the possible approaches to overcome such drawback is to fill the paraffin matrix with nanofillers that have much higher thermal conductivity coefficients [1,4]. To this end, it is highly desirable to understand the mechanisms by which the introduced nanoobjects affect the thermal conductivity of the original matrix. Such understanding is a key to design new materials with pre-defined thermal properties.

* Corresponding author.

E-mail address: a.gurtovenko@biosimu.org (A.A. Gurtovenko).

Advances in computer modeling have made it possible to perform a thorough analysis of a wide variety of the properties of materials *in silico*, including the thermal conductivity [5]. Computer modeling can be particularly useful in reducing the burden of the experimental work by screening and pre-selecting promising materials with desired properties. Depending on the resolution of a theoretical model, computer simulations can bring an insight into the structure and properties of materials on various scales, including the atomistic one. The models of high (atomic-scale) resolution offer the opportunity to understand the heat transport on a molecular level, as well as to reveal an underlying origin of the changes in the thermal conductivity upon filling the matrix with a nanofiller. Such an insight is unique for computer modeling and is not accessible from experimental measurements [5].

As far as the thermal conductivity is concerned, in molecular dynamics simulations two different approaches are commonly used. The first method is the equilibrium molecular dynamics (EMD); it is based on the Green-Kubo relation and takes into account the fluctuation-dissipation theorem to determine the heat flux [6–9]. The second approach is the non-equilibrium molecular dynamics (NEMD), in which the heat flux and the temperature gradient in a given direction are linked through the Fourier's law [10–12]. It was demonstrated that both EMD [6–8] and NEMD [10,13] methods can successfully be employed to compute the thermal conductivity coefficient in simulations. While it is generally accepted that both equilibrium and non-equilibrium methods are largely equivalent [9,14], a number of studies have reported discrepancies in the thermal conductivity evaluated by the two methods [6,15]. According to earlier studies, such discrepancies can partly be explained by the differences in simulation protocols [6,9,15,16]. Considerably less is known as to how the choice of a theoretical model (or, in other words, the interatomic interaction potentials and their parameters) affect the calculated thermal conductivity. In particular, the thermal conductivity is normally linked with the number of degrees of freedom, so that it is often believed that switching from the all-atom models to the united-atom ones leads to a drop in the thermal conductivity coefficient [17]. However, even if two models have the same resolution, they often can give different values of the thermal conductivity coefficients [15,16]. In general, among other factors, a force field is believed to have the greatest impact on the predicted thermal conductivity [18]. Thus, there is an obvious uncertainty regarding a proper choice of the theoretical model for calculating the thermal conductivity of a material at hand. In this paper we aim to resolve this uncertainty for a typical representative of organic phase-change materials.

The main goal of our study is to evaluate systematically how the choice of the theoretical model impacts the material's thermal conductivity calculated via both equilibrium and non-equilibrium methods. As a test system, here we chose to consider paraffin bulk samples. Paraffins, being relatively short n-alkanes, have a simple chemical structure and have been studied by computer simulations for decades. Paraffin is a typical representative of organic phase-change materials, so that the accurate evaluation of its thermal conductivity is highly desirable. Last but not least, paraffin is a crystallizable material, and this makes it possible to evaluate the thermal conductivity in both liquid and crystalline states. In our study we consider n-eicosane ($C_{20}H_{42}$), one of the most promising paraffins for the use in domestic heat storage devices [2]. The values of the thermal conductivity of n-eicosane samples were systematically evaluated for different models and critically compared with experimental data. To this end, we employed 10 different force fields of common use (both all-atom and united-atom ones). The thermal conductivity was evaluated for both liquid and solid states of n-eicosane samples with the use of EMD and NEMD methods. As we proceed to show, a proper choice of

a theoretical model for evaluating the thermal conductivity of organic phase-change materials (such as paraffins) can be a non-trivial task, as different force fields perform differently for liquid and solid states and when equilibrium and non-equilibrium methods are employed.

2. Methodology

2.1. Force fields and simulation details

We have performed molecular dynamics simulations of bulk samples of n-eicosane ($C_{20}H_{42}$). To study systematically the impact of a force field on the thermal conductivity, we considered 10 different atomistic force fields that are widely used for computer simulations of n-alkanes. These include both all-atom (GAFF [19], GAFF2 [20], OPLS-AA [21], L-OPLS-AA [22] and CHARMM36 [23]) and united-atom (TraPPE [24], NERD [25], OPLS-UA [26], PYS [27], and GROMOS [28]) force fields. For each force field the simulated paraffin samples consisted of 1000 n-eicosane chains. This amounted to the total number of 62,000 and 20,000 atoms in a system when all-atom and united-atom force fields were employed, respectively. Initial configurations of the n-eicosane samples were taken from our previous study [29]. For each force field we considered both liquid and crystalline states of the n-eicosane samples, see Fig. 1. The corresponding temperatures were set to 450 K and 250 K, respectively; the experimentally measured melting temperature of n-eicosane is 310 K [2]. Note that recently we showed [30] that the GROMOS force field is able to describe the crystalline phase of n-eicosane at $T = 250$ K, in contrast to ref [29] where the 1–4 Lennard-Jones interactions were not accounted for.

Both equilibrium and non-equilibrium molecular dynamics simulations were carried out with the use of the LAMMPS package (version from 15 Apr 2020) [31]. The equations of motion were numerically integrated with the use of the velocity-Verlet algorithm with a time step of 1.0 fs. The van der Waals interactions were truncated at a cut-off distance which was specific for each force field and ranged from 0.9 to 1.5 nm [29]. As all-atom models also include non-zero partial charges, the Ewald summation was used to handle the electrostatic interactions. The Coulomb interactions within the cut-off distance were calculated explicitly, while the Particle-Particle Particle-Mesh (PPPM) algorithm with a maximum relative error of 10^{-5} was employed at larger distances [32]. Following original parameterization [29], a correction in the interaction energy was applied beyond the cut-off distance for most considered force fields except CHARMM36 and PYS force fields. In all-atom simulations the bonds between carbon and hydrogen atoms were kept constant via the SHAKE algorithm [33]. In NVT simulations temperature was kept constant using the Nosé-Hoover thermostat with a time constant of 100 fs [34]. Periodic boundary conditions were applied along all three directions.

Prior actual simulations, all 10 atomistic force fields of n-eicosane were implemented into the LAMMPS package. In our previous study [29] we used the GROMACS suite [35] to assess how these force fields perform in terms of the structural and dynamic characteristics of n-eicosane over a wide temperature range. Therefore, to implement the n-eicosane force fields into the LAMMPS package, here we chose to transfer these models from GROMACS to LAMMPS with the use of the approach proposed in ref. [36]. To validate the GROMACS-to-LAMMPS force field conversion the absolute values of potential energy components, which were generated by both simulation packages, were directly compared to each other [37,38]. A detailed description of the conversion procedure is presented in the Supplementary Materials (Section S1 and Figs. S1–S5).

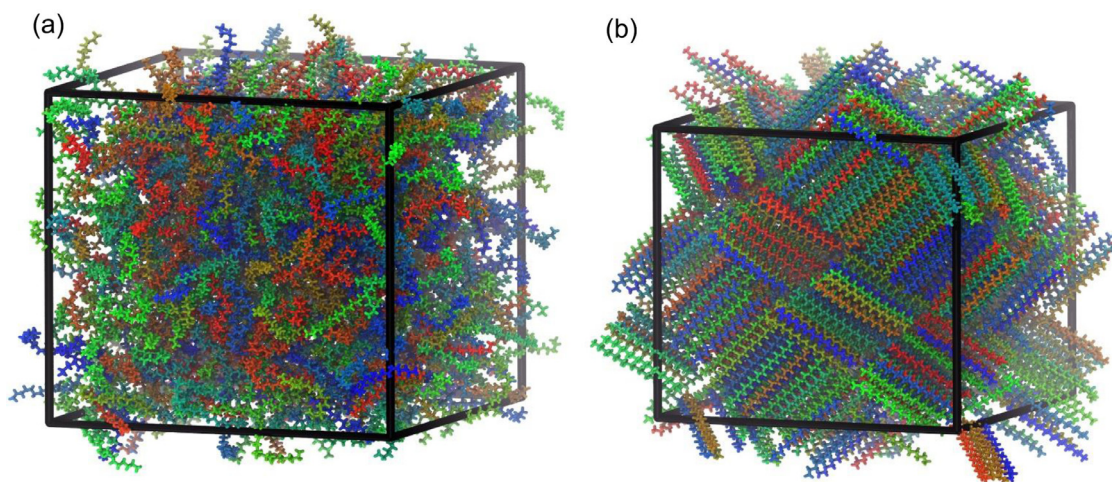


Fig. 1. Snapshots of n-eicosane samples in the liquid (a) and crystalline (b) states (the all-atom GAFF force field).

2.2. Calculation of thermal conductivity: equilibrium molecular dynamics

In equilibrium molecular dynamics (EMD) simulations the thermal conductivity κ is computed from the heat flux using the Green-Kubo relation. The total heat flux vector \vec{J} is given as [11]:

$$\vec{J} = \frac{1}{V} \left[\sum_i e_i \vec{v}_i + \frac{1}{2} \sum_{i < j} (\vec{f}_{ij} \cdot (\vec{v}_i + \vec{v}_j)) \vec{r}_{ij} \right], \quad (1)$$

where V is the volume of a simulation box, e_i is the total energy of the i^{th} atom with a velocity \vec{v}_i , \vec{f}_{ij} is the interatomic force between i^{th} and j^{th} atoms separated by a distance r_{ij} . The summation in Eq. (1) is performed over all atoms in the system. It should be noted that the second term in Eq. (1) includes contributions that come both from the non-bonded interactions (the van der Waals and Coulomb interactions), and from the bond, angle, proper and improper dihedral interactions, as well as from the internal constraint forces (if any). Once the total heat flux vector is known, the thermal conductivity coefficient κ can be evaluated by integrating the heat flux autocorrelation function $\langle \vec{J}(0) \vec{J}(t) \rangle$ [7,9]:

$$\kappa = \frac{V}{3k_B T^2} \int_0^\infty \langle \vec{J}(0) \cdot \vec{J}(t) \rangle dt, \quad (2)$$

where V is the volume of a simulation box, k_B is the Boltzmann constant, and T is the temperature.

The heat flux was calculated from 1 ns EMD simulations in the NVE ensemble with the use of the *heat/flux* procedure in the LAMMPS package. The heat flux was saved every 1 fs. The calculation of the autocorrelation functions of heat flux (HFACF) was performed using the correlation time of 10 ps [39]. To calculate HFACFs, we employed a recently modified formula for the virial, which properly accounts for the contributions that come from the valent angles and dihedrals to the heat flux [39,40]. The calculated HFACFs were used then for evaluating the thermal conductivity coefficient κ . For each force field, and for both liquid and crystalline phases (at $T = 250$ K and $T = 450$ K), the resulting values of the thermal conductivity coefficient were calculated by averaging over three independent n-eicosane samples.

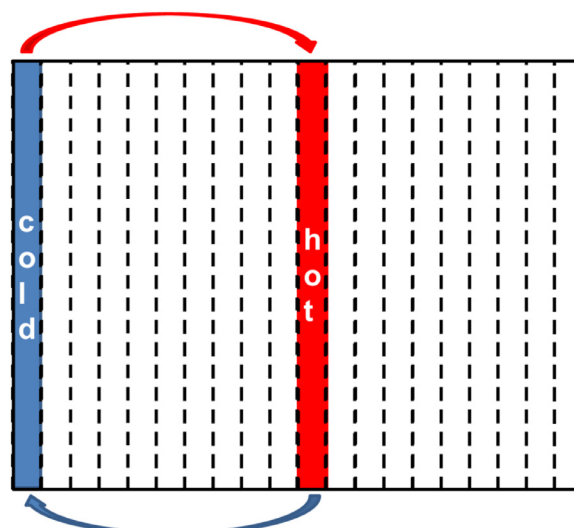


Fig. 2. A schematic representation of the exchange of the kinetic energy between the atoms in "hot" (red) and "cold" (blue) layers of a simulation box in NEMD simulations. Note that due to periodic boundary conditions another "cold" layer appears on the right-hand side of the box. Arrows show the directions of the exchange between the "hot" and "cold" layers. Dashed lines correspond to the division of a simulation box into the layers; in each layer the temperature is calculated via Eq. (5).

2.3. Calculation of thermal conductivity: non-equilibrium molecular dynamics

To calculate the thermal conductivity coefficient κ in the non-equilibrium molecular dynamics (NEMD) simulations, one needs to generate the heat flux in a simulation box. Here we use the so-called reverse NEMD approach, in which the heat flux is created in a system by an exchange of the kinetic energy between atoms located in different regions of a simulation box [17,41]. To do that, the simulation box is divided into a number of layers along e.g. the Z-direction and different temperatures are applied to the outermost (first and last) and central layers of a simulation box. Then the atoms with highest velocities from the "cold" layer exchange their velocities with the atoms with the lowest velocities from the "hot" layer, see Fig. 2. The velocity exchange is repeated with a certain frequency during NEMD simulations; this exchange preserves the total kinetic energy of a system. Once the temperature gradient

is established in the system, the thermal conductivity coefficient κ is calculated via the Fourier's law:

$$J_z = -\kappa (dT/dz), \quad (3)$$

where J_z is the heat flux along the heat flux direction (the Z-direction in this instance) and T is a temperature.

To calculate the thermal conductivity coefficient from NEMD simulations, the *thermal/conductivity* procedure of the LAMMPS package was used. A simulation box was divided into 20 layers [41]; the first layer was set to be the "cold" layer, while the central 11th layer – to be the "hot" layer, see Fig. 2. The heat flux J_z along the Z-direction was defined as the total kinetic energy transferred between atoms of the "cold" and "hot" layers per time and per surface area normal to the heat flux direction:

$$J_z = \frac{1}{2tA} \sum_{\text{transfers}} \frac{m}{2} (v_{\text{hot}}^2 - v_{\text{cold}}^2), \quad (4)$$

where t is time, A is the surface area, and v_{hot} and v_{cold} stand for the velocities of atoms with mass m in the "hot" and "cold" layers, respectively. To measure the temperature in each layer, the following relationship was used [12,17]:

$$T_{\text{slab}} = \frac{1}{3Nk_B} \left\langle \sum_{\substack{\text{atoms } i \\ \text{in a layer}}}^N m_i v_i^2 \right\rangle, \quad (5)$$

where N is the number of atoms in each layer, k_B is the Boltzmann constant, and the angular brackets indicate an averaging over a simulation time.

Actual NEMD simulations were carried out in two steps. First, 300 ps NVT simulation runs were performed for the temperature gradient to establish in a simulation box. By the end of these runs the temperature gradient did not change with time. Then, 100 ps NVT simulation runs were carried out to calculate the temperature gradient and the overall heat flux; these are used to compute the thermal conductivity coefficient via Eq. (3). The exchange of the velocities between the atoms in the "cold" and "hot" layers was repeated once per 10 steps (i.e. every 10 fs). Independent NEMD simulations were performed for X-, Y-, and Z-directions of the heat flux. The thermal conductivity coefficient κ was averaged over NEMD simulations with different directions of the heat flux, as well as over three independent n-icosane samples. Note that the thermal conductivity is normally computed from the NEMD simulations in the NVE ensemble. However, it turns out that using a constraints algorithm (SHAKE) for bonds between carbon and hydrogen atoms leads to a noticeable temperature drift. Therefore, we had to perform NVT simulations instead. The use of a thermostat was shown to have a little effect on the value of the thermal conductivity coefficient, the difference being less than 10% [17]. Our own estimates were in line with this finding.

3. Results and discussion

To assess the quality of any theoretical model, one needs, first, to set a reference for such a critical assessment. Here the thermal conductivity will be computed for two phase states of n-icosane samples via two computational methods with the use of 10 different force fields. Our computations will be performed at two temperatures: 250 K and 450 K, so that it is essential to have relevant experimental data at close temperatures. According to the experimental data, the melting temperature of n-icosane is 310 K [2]. For the crystalline samples of n-icosane most experiments were carried out at temperatures above 250 K. In particular, the

Table 1

The thermal conductivity coefficients κ of n-icosane bulk samples in the crystalline ($T = 250$ K) and in the liquid ($T = 450$ K) states, which are calculated via EMD simulations. The errors were estimated as standard errors over the last 500 ps of the trajectories. The experimental values of κ are also shown as a reference.

Force field	κ , W/(m•K)	
	$T=250$ K	$T=450$ K
CHARMM36	0.372 ± 0.002	0.197±0.002
GAFF	0.318 ± 0.002	0.143±0.001
GAFF2	0.448 ± 0.003	0.204±0.004
L-OPLS-AA	0.343 ± 0.001	0.190±0.001
OPLS-AA	0.482 ± 0.003	0.215±0.001
NERD	0.174 ± 0.001	0.092±0.003
OPLS-UA	0.215 ± 0.001	0.191±0.001
PYS	0.179 ± 0.001	0.079±0.003
TraPPE	0.205 ± 0.001	0.169±0.001
GROMOS	0.178 ± 0.001	0.083±0.001
Experiment	0.413 [45]	0.117 [46]

thermal conductivity scatters from 0.39 to 0.44 W/(m•K) in the temperature range of 275–283 K, depending on the measurement method used [42–44]. As the closest match to the simulation conditions is provided by the measurements at $T = 275$ K, we chose to use the corresponding experimental value of $\kappa = 0.413$ W/(m•K) [45] for comparison with computer modeling. As far as the n-icosane samples in the liquid state are concerned, the values of the thermal conductivity coefficients were found to be within the range 0.11 – 0.14 W/(m•K) [42]. For the sake of comparison, the experimental data of ref [46] will be used: $\kappa = 0.117$ W/(m•K) at $T = 453$ K.

3.1. Equilibrium molecular dynamics simulations

Prior the actual computation of the thermal conductivity from the EMD simulations, we estimated a characteristic time for the decay of the autocorrelation functions of heat flux (HFACF). In Fig. S6 we showed the HFACF as a function of time for both liquid and crystalline states, and for all 10 force fields considered. It is seen that in all cases the HFACF decays to zero over a time interval of 10 ps. It is noteworthy that, while the overall shapes of HFACF curves are similar for both the all-atom and the united-atom models, the HFACF decays are accompanied by stronger fluctuations for the all-atom force fields, which is a signature of the relaxation of explicit hydrogen atoms. Each n-icosane sample was simulated for 1 nanosecond. The last 10 ps of the trajectories were used to additionally prove that for all force fields the value of the thermal conductivity coefficient κ converges when the integration of the HFACF in Eq. (2) is performed over an interval of 10 ps, see Fig. S7.

With this information at hand, the thermal conductivity coefficient κ has been computed over 1 ns EMD trajectories with a time step of 10 ps for each force field and for both liquid and crystalline states, see Fig. S8. It is seen that the thermal conductivity of each system converges after ~500 ps, so that 1 ns trajectories are long enough to evaluate the thermal conductivity. The resulting values of the thermal conductivity coefficient κ were calculated by averaging over the last 500 ps of the EMD trajectories. These values for all systems considered are shown in Table 1.

The performance of each force field can be evaluated by a direct comparison of their predictions with the experimental data available. To simplify such analysis, for each force field we calculated a relative percentage deviation of a predicted value of the thermal conductivity coefficient κ_{sim} from the corresponding experimental value κ_{exp} : $(\kappa_{\text{sim}} - \kappa_{\text{exp}}) / \kappa_{\text{exp}} * 100\%$. The results are summarized in Fig. 3.

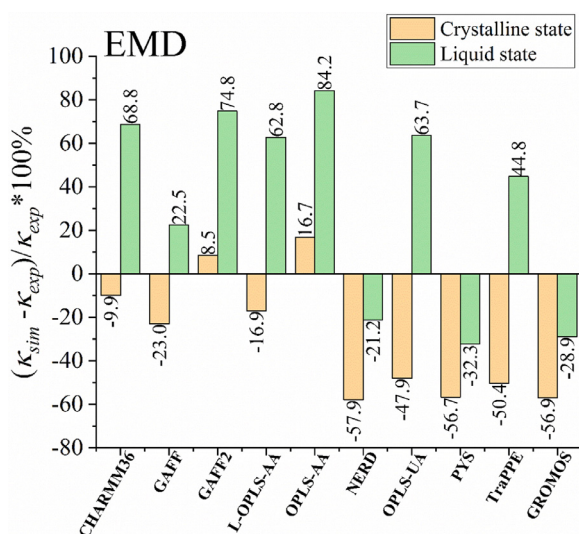


Fig. 3. The relative percentage deviation $(\kappa_{sim} - \kappa_{exp})/\kappa_{exp} * 100\%$ of computed thermal conductivity coefficients κ_{sim} from the experimental values for n-icosane samples in the crystalline ($T = 250$ K) and in the liquid ($T = 450$ K) states. Shown are the results for EMD simulations.

The results presented in Fig. 3 clearly show that the united-atom force fields of n-icosane perform poorly in the crystalline state: all considered united-atom models underestimate systematically the thermal conductivity. Interestingly, the relative percentage deviation from experimental data turns out to be very similar for all united-atom force fields and lies in the range of 48–58%, which implies that this feature could be inherent for the n-icosane models of lower resolution. It is known that in paraffin crystals the heat is transferred through vibrational waves of the crystal lattice. As shown in our earlier study [29], the n-icosane chains in the crystalline phase are more mobile in the case of united-atom models: the chains described within all-atom models have small partial charges, which additionally stabilize the crystal. The less stable crystal lattice leads to a scattering of phonons and, correspondingly, reduces the thermal conductivity. This can be a possible origin of the observed underestimation of κ_{sim} in crystalline phase when the united-atom models are used. The situation becomes better when the united-atom force fields are applied to the liquid state. The NERD, GROMOS, and PYS force fields still underestimate the thermal conductivity coefficient, but the deviation is significantly smaller (21–32%) as compared to that observed for crystals. The other two united-atom force fields (OPLS-UA and Trappe) overestimate considerably the experimental values of κ and perform much worse in the liquid state, see Fig. 3.

As far as the all-atom models are concerned, Fig. 3 shows that all of them perform rather well in the crystalline phase: the relative percentage deviation from experimental data does not exceed 23%. The best agreement with experiment at low temperatures is achieved when GAFF2 (8.5%) and CHARMM36 (9.9%) force fields are used. Interestingly, that the GAFF2 force field overestimates the experimental data, while the CHARMM36 underestimates it, see Fig. 3. In this regard, we found that the performance of different force fields in the crystalline phase could be linked to the difference in the chain stiffness of the corresponding computational models. The stiffness or the closely related local orientational mobility is mainly defined by bonded terms (bonds, angles, and dihedrals) of a force field, although the Lennard-Jones and Coulomb interactions also contribute. We calculated the characteristic relaxation time for the C–C bond vector for each force field and found that it correlates well with the thermal conductivity: the higher local orientational mobility, the lower the thermal con-

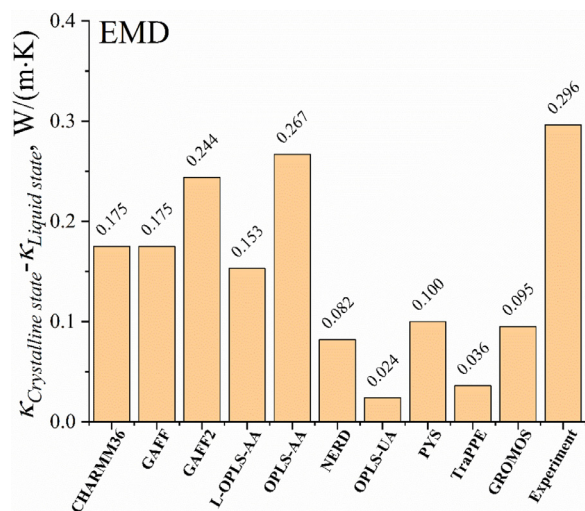


Fig. 4. The difference between the thermal conductivity coefficients of n-icosane samples in the crystalline ($T = 250$ K) and in the liquid ($T = 450$ K) states for different force fields. Shown are the results for EMD simulation, the experimental data are taken from refs [42,45,46].

ductivity, see Fig. S9, Fig. S10, and Table S2. This can be explained by the fact that scattering of phonons (responsible for a drop in the thermal conductivity) increases with the flexibility of paraffin chains. Note that this finding also holds for united-atom models. Correspondingly, the above-mentioned good performance of GAFF2 and CHARMM36 force fields in the crystalline state can be due to their more realistic chain stiffness compared to other models. Similarly, the GAFF2 force field overestimates the experimental value of the thermal conductivity because the chain stiffness in the frame of this model is too large (and vice versa for the CHARMM36 force field).

In turn, the performance of all-atom models in the liquid state is found to be considerably worse. Only the GAFF force field provides a reasonable match with experiment as it overestimates the thermal conductivity just by 22.5%. The overestimation of the values of κ for all other force fields with explicit hydrogen atoms turns out to be considerably larger and ranges from 63% to 84%, see Fig. 3. It is noteworthy that in the liquid phase the united-atom force field OPLS-UA gives the value of the thermal conductivity, which exceeds that computed for the all-atom force fields GAFF and L-OPLS-AA. This contradicts a generally accepted view that decreasing the resolution of a model leads to a drop of the thermal conductivity [17], highlighting thereby the fact that the relation between the force fields of different resolution can be more complex.

The ability of computational models to reproduce the thermal conductivity experimental data for the n-icosane samples can be considered from a different point of view. Experiments predict that the thermal conductivity coefficient of n-icosane in the crystalline phase exceeds considerably that in the liquid phase, see Table 1 and refs [45,46]. This is mainly due to the fact that the structure of liquids is much more disordered than the crystalline structure, which hinders the propagation of vibrational waves and, correspondingly, the heat transfer. Therefore, it is instructive to explore whether n-icosane models are able to reproduce this experimental feature. In Fig. 4 we present the differences between the thermal conductivity coefficients of crystalline and liquid phases for all considered force fields, as well as for the experiment.

First of all, it is seen that all considered models are able to reproduce qualitatively the experimentally observed trend: the thermal conductivity coefficients in the crystalline phase are found to be larger than those in the liquid phase. However, when it comes

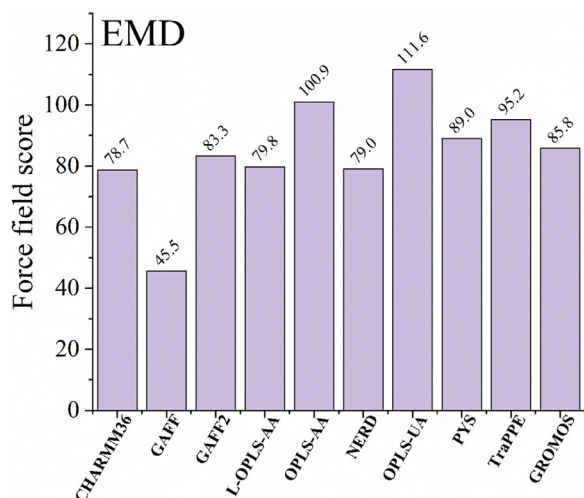


Fig. 5. The force field score calculated as a sum of the absolute values of relative percentage deviations $(\kappa_{sim}-\kappa_{exp})/\kappa_{exp} \cdot 100\%$ in both crystalline and liquid phases, for EMD simulations. The smaller the score, the better agreement with experiment.

to the quantitative comparison, it turns out that all the united-atom models fail to match the experimental situation, see Fig. 4. For instance, the difference in the thermal conductivity coefficients is almost vanishing for OPLS-UA and TraPPE force fields. The PYS force field, being the best performing united-atom force field here, provides the difference in the thermal conductivity of two phases, which is 3 times smaller than that measured in experiment. A much better agreement with experimental data is achieved with the use of the all-atom force fields. The best performance is observed in the case of OPLS-AA and GAFF2 force fields, the difference in values of κ being 0.267 W/(m•K) and 0.244 W/(m•K), respectively (cf. with experimental value of 0.296 W/(m•K)).

In order to rank the considered theoretical models in terms of their applicability for computing the thermal conductivity, it is highly desirable to have a cumulative quantity that would characterize the force field performance. Obviously, there is no unique way to achieve that. In this Section we discussed the performance of force fields in EMD simulations separately for crystalline and liquid phases, see Fig. 3. The above-mentioned cumulative quantity could summarize the force field performance for both phases. Therefore, as a force field score, here we chose to consider a sum of absolute values of relative percentage deviations of the thermal conductivity $(\kappa_{sim}-\kappa_{exp})/\kappa_{exp} \cdot 100\%$ in both crystalline and liquid phases.

As seen in Fig. 5, the best performance in the EMD simulations of n-eicosane is achieved by the all-atom GAFF force field. This force field shows reasonably small deviations from experiment, for both liquid and crystalline phases, giving rise to the smallest possible score among all 10 models (45.5%). Overall, the united-atom models perform somewhat worse than their all-atom counterparts; the corresponding score ranges between 79% (NERD) to 111.6% (OPLS-UA). The situation is a bit better for all-atom force fields. Apart from the GAFF force field, the score of the other four models scatter from 78.7% (CHARMM36) to 100.9% (OPLS-AA). Interestingly, that the score of the best performing united atom force field (NERD) practically coincides with the score of the all-atom CHARMM36 force field. Furthermore, the largest score (the worst performance) is observed for united-atom and all-atom versions of the OPLS force field, see Fig. 5. Note that the origin of high scores differs for models of different resolution. For all-atom force fields it comes mostly from the overestimation of the thermal conductivity in the liquid phase, while for united-atom models it is caused by too low values of κ in the crystalline phase.

Table 2

The thermal conductivity coefficients κ of n-eicosane bulk samples in the crystalline ($T = 250$ K) and in the liquid ($T = 450$ K) states, which are calculated via NEMD simulations. The standard errors were estimated upon averaging the values of κ over three directions of the heat flux and for three n-eicosane samples. The experimental values of κ are also shown as a reference.

Force field	κ , W/(m•K)	
	$T=250$ K	$T=450$ K
CHARMM36	0.336 ± 0.012	0.228 ± 0.002
GAFF	0.272 ± 0.012	0.183 ± 0.008
GAFF2	0.341 ± 0.017	0.246 ± 0.004
L-OPLS-AA	0.383 ± 0.010	0.244 ± 0.002
OPLS-AA	0.427 ± 0.012	0.282 ± 0.002
NERD	0.126 ± 0.005	0.079 ± 0.002
OPLS-UA	0.112 ± 0.012	0.137 ± 0.002
PYS	0.052 ± 0.001	0.076 ± 0.001
TraPPE	0.128 ± 0.007	0.142 ± 0.002
GROMOS	0.109 ± 0.003	0.075 ± 0.002
Experiment	0.413 [45]	0.117 [46]

3.2. Non-equilibrium molecular dynamics simulations

Turning now to the discussion of results of NEMD simulations, we recall that prior actual computations of the thermal conductivity one needs to establish a stable temperature gradient in a simulation box. To this end, the heat flux is created in a system during a 300 ps simulation run, see Section 2.3 for details. In Fig. S11 we present the corresponding temperature profiles as functions of the position in a simulation box along the direction of the heat flux. It is seen that for most systems the temperature reaches the linear regime, namely, it increases linearly from the “cold” layer to the “hot” layer in the middle of a simulation box, so that the temperature gradient can easily be computed from the slope of the temperature curve. The exceptions are observed for the crystalline samples when n-eicosane is described by the OPLS-UA, PYS, and GROMOS united-atom force fields. For these force fields the temperature-distance curves are characterized by two slopes, see Fig. S11(c). In line with earlier studies [12,47], the slope in the low-temperature domain was taken to calculate the temperature gradient (the linear approximation was applied within the intervals 0.5-3 nm and 5.5-7.5 nm in Fig. S11(c)).

Once the temperature gradient was established, the thermal conductivity was computed from a subsequent 100 ps NEMD run, see Section 2.3. The outcome of such calculations is presented in Table 2. Similar to the Section 3.1, Fig. 6 presents a relative percentage deviation $(\kappa_{sim}-\kappa_{exp})/\kappa_{exp} \cdot 100\%$ of the computed thermal conductivity coefficients with respect to the experimental values.

In NEMD simulations the united-atom models underestimate considerably the thermal conductivity in the crystalline state. The corresponding percentage deviation from the experimental data ranges between 69% and 87.4%. The united-atom models perform much better in the NEMD simulations when it comes to the liquid phases. OPLS-UA and TraPPE force fields give somewhat larger values of κ compared to those measured in experiment, while NERD, PYS, and GROMOS force fields underestimate the thermal conductivity coefficient. It is noteworthy because NEMD simulations of molecular liquids rarely underestimate the thermal conductivity [18]. Nevertheless, the relative percentage deviation in the liquid phase does not exceed 36%, which is much smaller as compared to that found for the n-eicosane samples in the crystalline phase.

In contrast to the united-atom models, the all-atom force fields provide a reasonable agreement with experimental data in the crystalline phase, see Fig. 6. The relative percentage deviations for this class of models are less than 35%. Most all-atom models un-

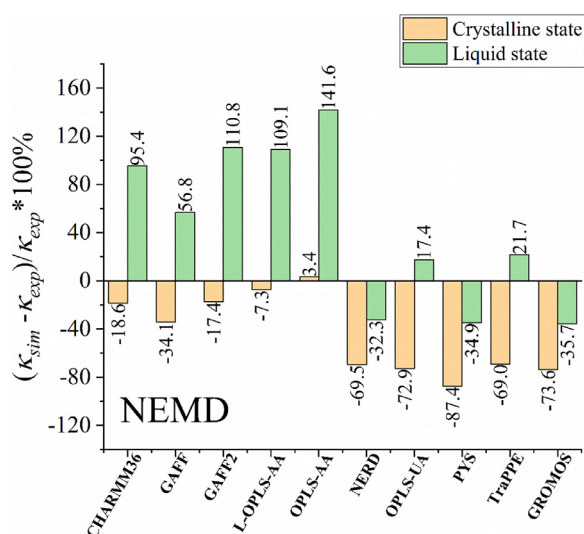


Fig. 6. The relative percentage deviation $(\kappa_{sim} - \kappa_{exp}) / \kappa_{exp} * 100\%$ of the computed thermal conductivity coefficients κ_{sim} from the experimental values for n-icosane samples in the crystalline ($T = 250$ K) and in the liquid ($T = 450$ K) states. Shown are the results for NEMD simulations.

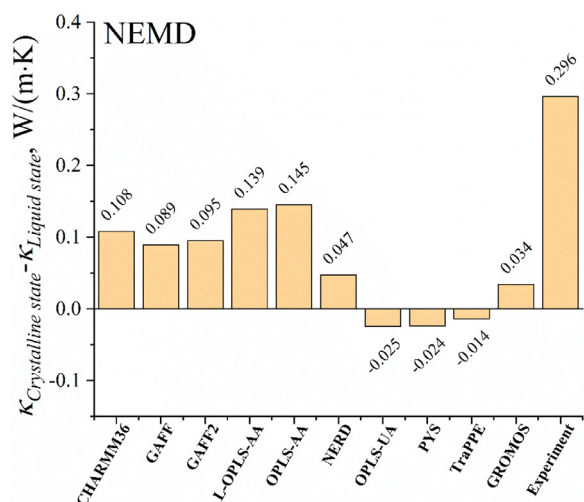


Fig. 7. The difference between thermal conductivity coefficients of n-icosane samples in crystalline ($T = 250$ K) and liquid ($T = 450$ K) states for different force fields. Shown are the results for NEMD simulations. The experimental data are taken from refs [42,45,46].

derestimate the experimental value of the thermal conductivity of paraffin crystals, except the OPLS-AA force field. Interestingly, this force field gives the best agreement with experiment (3.4%), along with its modified version L-OPLS-AA (-7.3%). The situation changes drastically when the all-atom models are used to study the liquid-state thermal conductivity in n-icosane samples. The best performing all-atom force field at high temperatures (GAFF) overestimates the experimental value of κ by 56.8%. The relative percentage deviations for other four models scatter from 95.4% (CHARMM36) to 141% (OPLS-AA), see Fig. 6. Furthermore, in NEMD simulations the thermal conductivity of a united-atom model is found to be always lower than that observed for an all-atom model in line with refs [17,18].

In the same fashion as for EMD simulations, in Fig. 7 we show the differences between the thermal conductivity coefficients of n-icosane samples in crystalline and liquid phases. In experiments the thermal conductivity of n-icosane in crystals exceeds considerably that for the liquid state [45,46]. As it is seen from Fig. 7,

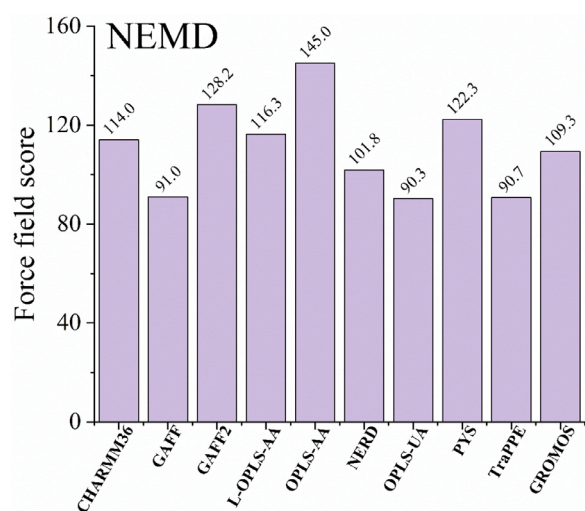


Fig. 8. The force field score calculated as a sum of the absolute values of relative percentage deviations $(\kappa_{sim} - \kappa_{exp}) / \kappa_{exp} * 100\%$ in both crystalline and liquid phases, for NEMD simulations. The smaller the score, the better agreement with experiment.

three united-atom models (OPLS-UA, PYS, and TrAPPE) fail to reproduce this experimental feature even qualitatively: the corresponding difference in κ is slightly negative. The other two united-atom models (NERD and GROMOS) show a correct trend, but the absolute values of the difference in κ for crystalline and liquid states are of an order of magnitude smaller than that observed in experiment. The situation is considerably better for the models with explicit hydrogen atoms. All of them reproduce an experimentally observed increase in the thermal conductivity upon crystallization. However, even the force fields that demonstrate the best performance here (OPLS-AA and L-OPLS-AA) underestimate the difference in the thermal conductivity by a factor of 2, see Fig. 7.

We conclude this Section by considering the overall score of force fields in NEMD simulations. In line with Section 3.1, the force field score was calculated as a sum of the absolute values of relative percentage deviations of the thermal conductivity $(\kappa_{sim} - \kappa_{exp}) / \kappa_{exp} * 100\%$ in crystalline and liquid phases. As seen in Fig. 8, the smallest score (the best performance) in NEMD simulations is found for united-atom force fields OPLS-UA (90.3%) and TrAPPE (90.7%) and for the all-atom force field GAFF (91%). Remarkably, the score of all other force fields exceeds 100%. The overall performance of united-atom models in NEMD simulations turns out to be slightly better, as the models with explicit hydrogen atoms overestimate the thermal conductivity in the liquid state to a significant degree, see Fig. 6.

3.3. Comparison of EMD and NEMD simulations

As already discussed in the Introduction, it is generally accepted that both equilibrium and non-equilibrium MD simulations are equivalent in terms of computing the thermal conductivity coefficient [9,14]. On the other hand, some reports have demonstrated a pronounced sensitivity of the computed values of thermal conductivity coefficients to the theoretical model (the force field) employed [17,18]. As we showed in Sections 3.1 and 3.2, the use of different force fields for describing n-icosane bulk samples indeed affects drastically the thermal conductivity computed via EMD and NEMD simulations. However, such an effect may differ significantly for equilibrium and non-equilibrium methods, giving rise to the corresponding differences in the thermal conductivity coefficients

computed by both methods. These differences will be summarized in this Section.

Prior actual comparison of the outcomes of EMD and NEMD simulations, one has to make an important remark regarding possible size effects. As virtually any molecular dynamics simulations, the EMD and NEMD methods used in our study could suffer from the effects of a finite size. In the case of EMD, the size effects are often considered to be relatively small. In particular, it was shown that the system size in EMD simulations of bulk samples of n-dodecane, n-eicosane and n-triacontane affects only slightly the calculated values of the thermal conductivity coefficient [48,49]. As far as the NEMD simulations are concerned, they are believed to be more sensitive to the system size as compared to the EMD method [50]. In the case of molecular liquids, it was shown that the size effects in NEMD simulations can be avoided if systems of some thousand molecules with a box length of several nanometers are considered [18] (we note that this could not be enough in NEMD simulations of oligomers or polymers). For the paraffin bulk samples studied here, we considered relatively large systems. Each system consisted of 1000 n-eicosane chains, which amounted to 62,000 atoms for all-atom models; the average length of a cubic simulation box was around 7.5 nm and 8.5 nm for the samples in crystalline and liquid phases, respectively. Because 10 different force fields have been considered, as well as three independent configurations for each system and two phase states of n-eicosane samples, varying the system size for all the considered systems would be computationally prohibitive (especially in view of a relatively low performance of the software package used for computations, see Table S1). Therefore, in this Section we chose to report a comparison between EMD and NEMD methods for the above-mentioned system sizes. It has to be stressed that such a comparison should be taken with caution in view of the possible size effects.

The absolute values of the thermal conductivity coefficients for EMD and NEMD simulations are summarized in Fig. S12. However, it is much more instructive to discuss the relative percentage deviation $(\kappa_{sim} - \kappa_{exp})/\kappa_{exp} * 100\%$ of computed thermal conductivity coefficients from experimental values, see Fig. 9. For n-eicosane samples in the crystalline state both EMD and NEMD simulations underestimate considerably the thermal conductivity when united-atom models are used. Although the EMD method provides a better match with experiment at low temperatures, the general trend is the same for both methods, see Fig. 9(a). As for the force fields with explicit hydrogen atoms, they perform much better in crystals than their united-atom counterparts, regardless of which MD method was used. However, the relation between the outcomes of EMD and NEMD simulations is less certain for all-atom models. While CHARMM36, GAFF, and GAFF2 force fields give a better agreement with experiment in EMD simulations, the NEMD method turns out to be more preferable for all-atom representatives of the OPLS force field family, see Fig. 9(a). Overall, the best match (3.4%) with experimental data at low temperatures is observed when the OPLS-AA force field is used in NEMD simulations.

Turning now to the thermal conductivity of n-eicosane samples in the liquid phase, one can conclude that for both MD methods united-atom models perform much better than the models with explicit hydrogen atoms, see Fig. 9(b). As for the comparison of the outcome of united-atom models in the liquid phase, we observe different trends for different force fields. NEMD simulations in conjunction with NERD, PYS, and GROMOS force fields give slightly larger deviations from experiment as compared to EMD simulations. In contrast, the OPLS-UA and TraPPE force fields perform much better when NEMD simulations are used. Furthermore, NEMD simulations with the OPLS-UA force field give the best agreement (17.4%) with experimental data in the liquid phase among all the model considered, see Fig. 9(b). In turn, all-atom

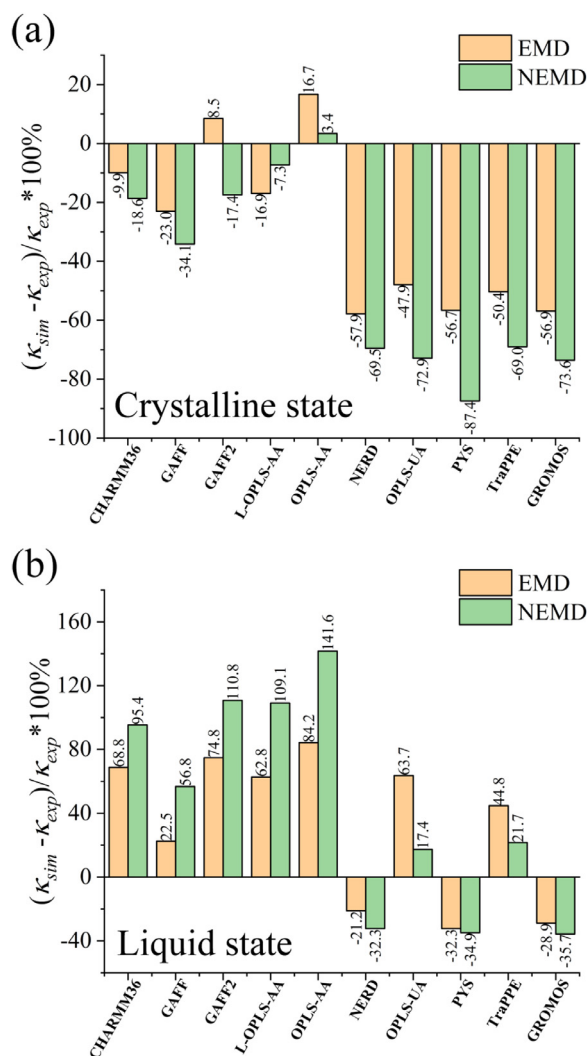


Fig. 9. The relative percentage deviation $(\kappa_{sim} - \kappa_{exp})/\kappa_{exp} * 100\%$ of computed thermal conductivity coefficients κ_{sim} from the experimental values for n-eicosane samples in the crystalline (a) and in the liquid (b) states. Shown are the results for both EMD and NEMD simulations.

models overestimate the thermal conductivity for both EMD and NEMD methods. Interestingly, the NEMD method gives systematically larger deviations from experiment at high temperatures for each all-atom force field.

In Fig. 10 we plotted the differences between the thermal conductivity coefficients of n-eicosane samples in crystalline and liquid phases as computed by EMD and NEMD simulations. It is seen that the EMD method provides a better agreement with experimental data as compared to NEMD simulations for all force fields considered. In other words, NEMD simulations systematically underestimate the experimentally observed difference in the values of κ of the two phases of n-eicosane samples. What is more, for some united-atom models (OPLS-UA, PYS, and TraPPE) the NEMD method predicts that the thermal conductivity is higher in the liquid phase, which contradicts with experiment.

Finally, in Fig. 11 we present the overall score of all considered force fields in both EMD and NEMD simulations. As one can see, most force fields perform considerably better in EMD simulations (at least for the considered size of a simulation box). This is essentially the case for the all-atom models. The best performance among the all-atom models is observed for the GAFF force field. Remarkably, this conclusion holds for both EMD and NEMD

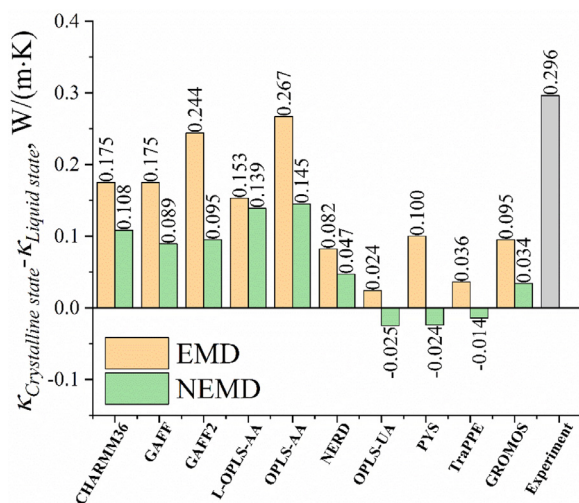


Fig. 10. The difference between the thermal conductivity coefficients of n-icosane samples in crystalline ($T = 250$ K) and liquid ($T = 450$ K) states for different force fields. Shown are the results for both EMD and NEMD simulations. The experimental data are taken from refs [42,45,46].

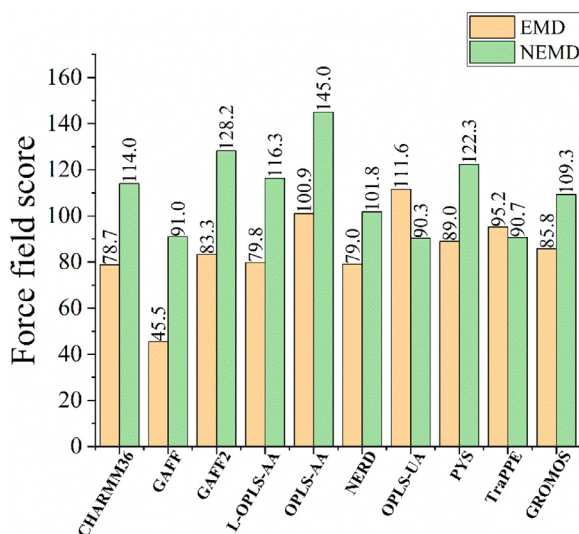


Fig. 11. The force field score calculated as a sum of the absolute values of relative percentage deviations $(\kappa_{sim} - \kappa_{exp})/\kappa_{exp} * 100\%$ in crystalline and liquid phases. Shown are the results for both EMD and NEMD simulations. The smaller the score, the better agreement with experiment.

simulations, i.e. is method independent. Nevertheless, it should be kept in mind that for the GAFF model the force field score in EMD simulations is twice smaller (better) than that in NEMD calculations. Based on the force field scores presented in Fig. 11, the CHARMM36 and L-OPLS-AA all-atom models could be considered as a second option in addition to the GAFF force field. As for united-atom models, we have two instances in which NEMD simulations outperform EMD ones: OPLS-UA and TraPPE force fields, see Fig. 11. The rest of the united-atom force fields follow the same pattern as their high-resolution counterparts: the score in NEMD simulations is considerably larger (worse) than the one observed for the EMD method.

4. Conclusions

The accurate evaluation of the thermal conductivity from *in silico* modeling is critical for a rational design of new materials with pre-defined thermal properties. In particular, the ability to predict correctly the thermal conductivity is highly desirable for or-

ganic phase-change materials which have a great potential for the use in domestic heat storage systems. To this end, we have performed EMD and NEMD simulations of n-icosane bulk samples in crystalline ($T=250$ K) and liquid ($T=450$ K) states with the use of 10 atomistic force fields, both all-atom (CHARMM36, GAFF, GAFF2, OPLS-AA, and L-OPLS-AA) and united-atom (NERD, OPLS-UA, PYS, TraPPE, and GROMOS) ones.

We found that in the crystalline phase all united-atom force fields systematically underestimate the thermal conductivity and perform much worse than the models with the explicit hydrogen atoms in both EMD and NEMD simulations. This difference between the models of high and low resolution could be explained by the fact that n-icosane chains in the crystalline phase are known to be more mobile when united-atom models are used [29]. The latter lack partial charges of explicit hydrogen atoms, which additionally stabilize the crystal in the case of all-atom models. This higher mobility can dissipate vibrational waves in the crystal lattice and correspondingly hinder the heat transfer, thereby reducing the thermal conductivity. The best performance in the crystalline state is provided by GAFF2 and CHARMM36 force fields (EMD simulations) and by OPLS-AA and L-OPLS-AA force fields (NEMD simulations).

For the n-icosane samples in the liquid phase we witness the opposite trend. All-atom force fields perform worse than their united-atom counterparts and overestimate considerably the experimental data in both EMD and NEMD simulations with the exception of the GAFF force field (EMD simulations). Among united-atom models, the best performance in the liquid phase is achieved with the use of the NERD force field (EMD simulations) and of OPLS-UA and TraPPE force fields (NEMD simulations). In general, the all-atom systems consist of a significantly larger number of atoms as compared to the united-atom counterpart, and are characterized, therefore, by shorter free paths between atoms. This could explain why all-atom models overestimate the thermal conductivity in the highly disordered liquid state: the shorter phonon free path, the lower scattering of phonons.

Most force fields were shown to reproduce qualitatively the experimentally observed increase of the thermal conductivity upon crystallization [45,46], except united-atom models OPLS-UA, PYS, and TraPPE (NEMD simulations). However, when compared quantitatively, united-atom models fail to match the experimental difference in the thermal conductivity of two phases. All-atom models demonstrate a much better agreement with experiment, especially when the EMD method is used. The best match is observed for OPLS-AA and GAFF2 force fields (EMD simulations).

Finally, we characterized each force field by an overall score which accumulated the deviations from experiment for both crystalline and liquid states. It turns out that EMD simulations systematically outperform NEMD counterparts with just two exceptions: united-atom force fields OPLS-UA and TraPPE. Therefore, the EMD method would be more preferable for computing the thermal conductivity of n-icosane (at least for a simulation box with a length of ~ 8 nm). The best performance among all 10 force fields of n-icosane is found for the all-atom GAFF force field; remarkably, this conclusion is independent of the MD method employed. As for the united-atom models, the NERD force field shows the best performance (EMD simulations).

Overall, our study clearly demonstrates that the choice of a theoretical model has a strong impact on the computed values of the thermal conductivity coefficients of organic phase-change materials. Even for such relatively simple compounds as paraffins (n-alkanes), this impact can differ considerably in equilibrium and non-equilibrium simulations as well as in crystalline and liquid samples.

Declaration of Competing Interest

The authors declare no conflicts of interest.

CRediT authorship contribution statement

Victor M. Nazarychev: Methodology, Software, Validation, Investigation, Formal analysis, Writing - original draft, Visualization. **Artyom D. Glova:** Validation, Investigation, Formal analysis, Writing - review & editing, Visualization. **Igor V. Volgin:** Validation, Investigation, Formal analysis, Writing - review & editing. **Sergey V. Larin:** Methodology, Investigation, Writing - review & editing. **Alexey V. Lyulin:** Conceptualization, Methodology, Writing - review & editing, Supervision. **Sergey V. Lyulin:** Conceptualization, Methodology, Writing - review & editing, Supervision, Funding acquisition. **Andrey A. Gurtovenko:** Conceptualization, Methodology, Validation, Writing - review & editing, Supervision, Project administration, Funding acquisition.

Acknowledgments

This work was supported by the Russian Science Foundation (State Agreement No. 19-13-00178). Computer simulations were performed using the computational resources of the Institute of Macromolecular Compounds, Russian Academy of Sciences, the equipment of the shared research facilities of HPC computing resources at Lomonosov Moscow State University, the resources of the Federal collective usage center "Complex for Simulation and Data Processing for Mega-science Facilities" at the NRC "Kurchatov Institute" (<http://ckp.nrcki.ru/>), and supercomputers at Joint Supercomputer Center of the Russian Academy of Sciences (JSCC RAS).

Supplementary materials

Supplementary material associated with this article can be found, in the online version, at [doi:10.1016/j.ijheatmasstransfer.2020.120639](https://doi.org/10.1016/j.ijheatmasstransfer.2020.120639).

References

- [1] H. Chen, V.V. Ginzburg, J. Yang, Y. Yang, W. Liu, Y. Huang, L. Du, B. Chen, Thermal conductivity of polymer-based composites: fundamentals and applications, *Prog. Polym. Sci.* 59 (2016) 41–85, doi:10.1016/j.progpolymsci.2016.03.001.
- [2] A. Sharma, V.V. Tyagi, C.R. Chen, D. Buddhi, Review on thermal energy storage with phase change materials and applications, *Renew. Sustain. Energy Rev.* 13 (2009) 318–345, doi:10.1016/j.rser.2007.10.005.
- [3] H. Peng, D. Zhang, X. Ling, Y. Li, Y. Wang, Q. Yu, X. She, Y. Li, Y. Ding, N-alkanes phase change materials and their microencapsulation for thermal energy storage: a critical review, *Energy Fuels* 32 (2018) 7262–7293, doi:10.1021/acs.energyfuels.8b01347.
- [4] K. Tumuluri, J.L. Alvarado, H. Taherian, C. Marsh, Thermal performance of a novel heat transfer fluid containing multiwalled carbon nanotubes and microencapsulated phase change materials, *Int. J. Heat Mass Transf.* 54 (2011) 5554–5567, doi:10.1016/j.ijheatmasstransfer.2011.07.031.
- [5] X. Xu, J. Chen, J. Zhou, B. Li, Thermal conductivity of polymers and their nanocomposites, *Adv. Mater.* 30 (2018) 1–10, doi:10.1002/adma.201705544.
- [6] R. Rastgarkafshgarkolaei, Y. Zeng, J.M. Khodadadi, A molecular dynamics study of the effect of thermal boundary conductance on thermal transport of ideal crystal of n-alkanes with different number of carbon atoms, *J. Appl. Phys.* 119 (2016) 205107, doi:10.1063/1.4952411.
- [7] C. Lin, Z. Rao, Thermal conductivity enhancement of paraffin by adding boron nitride nanostructures: a molecular dynamics study, *Appl. Therm. Eng.* 110 (2017) 1411–1419, doi:10.1016/j.applthermaleng.2016.09.065.
- [8] S. Srinivasan, M.S. Diallo, S.K. Saha, O.A. Abass, A. Sharma, G. Balasubramanian, Effect of temperature and graphite particle fillers on thermal conductivity and viscosity of phase change material n-icosane, *Int. J. Heat Mass Transf.* 114 (2017) 318–323, doi:10.1016/j.ijheatmasstransfer.2017.06.081.
- [9] P.K. Schelling, S.R. Phillpot, P. Keblinski, Comparison of atomic-level simulation methods for computing thermal conductivity, *Phys. Rev. B - Condens. Matter Mater. Phys.* 65 (2002) 1–12, doi:10.1103/PhysRevB.65.144306.
- [10] Y. Wang, C. Yang, Y.W. Mai, Y. Zhang, Effect of non-covalent functionalisation on thermal and mechanical properties of graphene-polymer nanocomposites, *Carbon* 102 (2016) 311–318, doi:10.1016/j.carbon.2016.02.069.
- [11] T. Zhang, T. Luo, Role of chain morphology and stiffness in thermal conductivity of amorphous polymers, *J. Phys. Chem. B* 120 (2016) 803–812, doi:10.1021/acs.jpcc.5b09955.
- [12] F. Müller-Plathe, A simple nonequilibrium molecular dynamics method for calculating the thermal conductivity, *J. Chem. Phys.* 106 (1997) 6082–6085, doi:10.1063/1.473271.
- [13] Y.-R. Huang, P.-H. Chuang, C.-L. Chen, Molecular-dynamics calculation of the thermal conduction in phase change materials of graphene paraffin nanocomposites, *Int. J. Heat Mass Transf.* 91 (2015) 45–51, doi:10.1016/j.ijheatmasstransfer.2015.07.110.
- [14] H. Matsubara, G. Kikugawa, M. Ishikiriyama, S. Yamashita, T. Ohara, Equivalence of the EMD- and NEMD-based decomposition of thermal conductivity into microscopic building blocks, *J. Chem. Phys.* 147 (2017) 114104, doi:10.1063/1.4990593.
- [15] R.N. Salaway, L.V. Zhigilei, Molecular dynamics simulations of thermal conductivity of carbon nanotubes: resolving the effects of computational parameters, *Int. J. Heat Mass Transf.* 70 (2014) 954–964, doi:10.1016/j.ijheatmasstransfer.2013.11.065.
- [16] M. Vohra, A.Y. Nobakht, S. Shin, S. Mahadevan, Uncertainty quantification in non-equilibrium molecular dynamics simulations of thermal transport, *Int. J. Heat Mass Transf.* 127 (2018) 297–307, doi:10.1016/j.ijheatmasstransfer.2018.07.073.
- [17] M. Zhang, E. Lussetti, L.E.S. De Souza, F. Müller-Plathe, Thermal conductivities of molecular liquids by reverse nonequilibrium molecular dynamics, *J. Phys. Chem. B* 109 (2005) 15060–15067, doi:10.1021/jp0512255.
- [18] E.A. Algaer, F. Müller-Plathe, Molecular dynamics calculations of the thermal conductivity of molecular liquids, polymers, and carbon nanotubes, *Soft Mater.* 10 (2012) 42–80, doi:10.1080/1539445X.2011.599699.
- [19] J. Wang, R.M. Wolf, J.W. Caldwell, P.A. Kollman, D.A. Case, Development and testing of a general amber force field, *J. Comput. Chem.* 25 (2004) 1157–1174, doi:10.1002/jcc.20035.
- [20] D. Vassetti, M. Pagliai, P. Procacci, Assessment of GAFF2 and OPLS-AA general force fields in combination with the water models TIP3P, SPCE, and OPC3 for the solvation free energy of druglike organic molecules, *J. Chem. Theo. Comput.* 15 (2019) 1983–1995, doi:10.1021/acs.jctc.8b01039.
- [21] W.L. Jorgensen, D.S. Maxwell, J. Tirado-Rives, Development and testing of the OPLS all-atom force field on conformational energetics and properties of organic liquids, *J. Am. Chem. Soc.* 118 (1996) 11225–11236, doi:10.1021/ja9621760.
- [22] S.W.I. Siu, K. Pluhackova, R.A. Böckmann, Optimization of the OPLS-AA force field for long hydrocarbons, *J. Chem. Theo. Comput.* 8 (2012) 1459–1470, doi:10.1021/ct200908r.
- [23] J.B. Klauda, R.M. Venable, J.A. Freites, J.W. O'Connor, D.J. Tobias, C. Mondragon-Ramirez, I. Vorobyov, A.D. MacKerell, R.W. Pastor, Update of the CHARMM all-atom additive force field for lipids: validation on six lipid types, *J. Phys. Chem. B* 114 (2010) 7830–7843, doi:10.1021/jp101759q.
- [24] M.G. Martin, J.I. Siepmann, Predicting multicomponent phase equilibria and free energies of transfer for alkanes by molecular simulation, *J. Am. Chem. Soc.* 119 (1997) 8921–8924, doi:10.1021/ja964218q.
- [25] S.K. Nath, F.A. Escobedo, J.J. De Pablo, On the simulation of vapor-liquid equilibria for alkanes, *J. Chem. Phys.* 108 (1998) 9905–9911, doi:10.1063/1.476429.
- [26] W.L. Jorgensen, J.D. Madura, C.J. Swenson, Optimized intermolecular potential functions for liquid hydrocarbons, *J. Am. Chem. Soc.* 106 (1984) 6638–6646, doi:10.1021/ja00334a030.
- [27] W. Paul, D.Y. Yoon, G.D. Smith, An optimized united atom model for simulations of polymethylene melts, *J. Chem. Phys.* 103 (1995) 1702–1709, doi:10.1063/1.469740.
- [28] L.D. Schuler, J. Daura, W.F. Van Gunsteren, An improved GROMOS96 force field for aliphatic hydrocarbons in the condensed phase, *J. Comput. Chem.* 22 (2001) 1205–1218, doi:10.1002/jcc.1078.
- [29] A.D. Glova, I.V. Volgin, V.M. Nazarychev, S.V. Larin, S.V. Lyulin, A.A. Gurtovenko, Toward realistic computer modeling of paraffin-based composite materials: critical assessment of atomic-scale models of paraffins, *RSC Adv.* 9 (2019) 38834–38847, doi:10.1039/C9RA07325F.
- [30] I.V. Volgin, A.D. Glova, V.M. Nazarychev, S.V. Larin, S.V. Lyulin, A.A. Gurtovenko, Correction: toward realistic computer modeling of paraffin-based composite materials: critical assessment of atomic-scale models of paraffins, *RSC Adv.* 10 (2020) 31316–31317, doi:10.1039/D0RA090087G.
- [31] S. Plimpton, Fast parallel algorithms for short-range molecular dynamics, *J. Comp. Phys.* 117 (1995) 1–19, doi:10.1006/jcph.1995.1039.
- [32] R.W. Hockney, J.W. Eastwood, *Computer Simulation Using Particles*, Adam Hilger, NY, 1989.
- [33] J.-P. Ryckaert, G. Cicciotti, H.J. Berendsen, Numerical integration of the cartesian equations of motion of a system with constraints: molecular dynamics of n-alkanes, *J. Comput. Phys.* 23 (1977) 327–341, doi:10.1016/0021-9991(77)90098-5.
- [34] S. Nosé, A unified formulation of the constant temperature molecular dynamics methods, *J. Chem. Phys.* 81 (1984) 511–519, doi:10.1063/1.447334.
- [35] D. Van Der Spoel, E. Lindahl, B. Hess, G. Groenhof, A.E. Mark, H.J.C. Berendsen, GROMACS: fast, flexible, and free, *J. Comput. Chem.* 26 (2005) 1701–1718, doi:10.1002/jcc.20291.

- [36] M.R. Shirts, C. Klein, J.M. Swails, J. Yin, M.K. Gilson, D.L. Mobley, D.A. Case, E.D. Zhong, Lessons learned from comparing molecular dynamics engines on the SAMPL5 dataset, *J. Comput.-Aid. Mol. Des.* 31 (2017) 147–161, doi:[10.1007/s10822-016-9977-1](https://doi.org/10.1007/s10822-016-9977-1).
- [37] V.H. Rusu, V.A.C. Horta, B.A.C. Horta, R.D. Lins, R. Baron, MDWiZ: a platform for the automated translation of molecular dynamics simulations, *J. Mol. Graph. Model.* 48 (2014) 80–86, doi:[10.1016/j.jmkgm.2013.12.006](https://doi.org/10.1016/j.jmkgm.2013.12.006).
- [38] H. Chávez Thielemann, A. Cardellini, M. Fasano, L. Bergamasco, M. Alberghini, G. Ciorra, E. Chiavazzo, P. Asinari, From GROMACS to LAMMPS: GRO2LAM, *J. Mol. Model.* 25 (2019) 147, doi:[10.1007/s00894-019-4011-x](https://doi.org/10.1007/s00894-019-4011-x).
- [39] D. Surblyš, H. Matsubara, G. Kikugawa, T. Ohara, Application of atomic stress to compute heat flux via molecular dynamics for systems with many-body interactions, *Phys. Rev. E* 99 (2019) 051301, doi:[10.1103/PhysRevE.99.051301](https://doi.org/10.1103/PhysRevE.99.051301).
- [40] P. Boone, H. Babaei, C.E. Wilmer, Heat flux for many-body interactions: corrections to LAMMPS, *J. Chem. Theo. Comput.* 15 (2019) 5579–5587, doi:[10.1021/acs.jctc.9b00252](https://doi.org/10.1021/acs.jctc.9b00252).
- [41] F. Müller-Plathe, A simple nonequilibrium molecular dynamics method for calculating the thermal conductivity, *J. Chem. Phys.* 106 (2002) 6082–6085, doi:[10.1063/1.473271](https://doi.org/10.1063/1.473271).
- [42] R.M. Al Ghossein, M.S. Hossain, J.M. Khodadadi, Experimental determination of temperature-dependent thermal conductivity of solid eicosane-based silver nanostructure-enhanced phase change materials for thermal energy storage, *Int. J. Heat Mass Transf.* 107 (2017) 697–711, doi:[10.1016/j.ijheatmasstransfer.2016.11.059](https://doi.org/10.1016/j.ijheatmasstransfer.2016.11.059).
- [43] P.C. Stryker, E.M. Sparrow, Application of a spherical thermal conductivity cell to solid n-eicosane paraffin, *Int. J. Heat Mass Transf.* 33 (1990) 1781–1793, doi:[10.1016/0017-9310\(90\)90212-D](https://doi.org/10.1016/0017-9310(90)90212-D).
- [44] X. Fang, L. Fan, Q. Ding, X. Wang, X. Yao, J. Hou, Z. Yu, G.-H. Cheng, Y.-C. Hu, K.-F. Cen, Increased thermal conductivity of eicosane-based composite phase change materials in the presence of graphene nanoplatelets, *Energy Fuels* 27 (2013) 4041–4047, doi:[10.1021/ef400702a](https://doi.org/10.1021/ef400702a).
- [45] E.I. Griggs, D.W. Yarbrough, Thermal conductivity of solid unbranched alkanes from n-hexadecane to n-eicosane, in: *proceedings of the Southeastern seminar on thermal sciences, North Carolina State University, 1978*, pp. 256–257.
- [46] Y.L. Rastorguev, G.F. Bogatov, B.A. Grigor'ev, Thermal conductivity of higher n-alkanes, *Chem. Technol. Fuels. Oils* 10 (1974) 728–732, doi:[10.1007/BF00717208](https://doi.org/10.1007/BF00717208).
- [47] H. Matsubara, G. Kikugawa, T. Bessho, T. Ohara, Evaluation of thermal conductivity and its structural dependence of a single nanodiamond using molecular dynamics simulation, *Diamond Relat. Mater.* 102 (2020) 107669, doi:[10.1016/j.diamond.2019.107669](https://doi.org/10.1016/j.diamond.2019.107669).
- [48] H. Babaei, P. Keblinski, J.M. Khodadadi, Thermal conductivity enhancement of paraffins by increasing the alignment of molecules through adding CNT/graphene, *Int. J. Heat Mass Transf.* 58 (2013) 209–216, doi:[10.1016/j.ijheatmasstransfer.2012.11.013](https://doi.org/10.1016/j.ijheatmasstransfer.2012.11.013).
- [49] Y. Zeng, J.M. Khodadadi, Molecular dynamics simulations of the crystallization process of n-alkane mixtures and the resulting thermal conductivity, *Energy Fuels* 32 (2018) 11253–11260, doi:[10.1021/acs.energyfuels.8b02500](https://doi.org/10.1021/acs.energyfuels.8b02500).
- [50] Z. Wang, X. Ruan, On the domain size effect of thermal conductivities from equilibrium and nonequilibrium molecular dynamics simulations, *J. Appl. Phys.* 121 (2017) 044301, doi:[10.1063/1.4974884](https://doi.org/10.1063/1.4974884).